

RESEARCH ARTICLE

Cortico-basal white matter alterations occurring in Parkinson's disease

Bethany R. Isaacs^{1,2*}, Anne C. Trutti^{1,3}, Esther Pelzer^{4,5}, Marc Tittgemeyer^{4,5}, Yasin Temel², Birte U. Forstmann¹, Max C. Keuken¹

1 Integrative Model-based Cognitive Neuroscience research unit, University of Amsterdam, Amsterdam, the Netherlands, **2** Department of Neurosurgery, Maastricht University Medical Centre, Maastricht, The Netherlands, **3** Cognitive Psychology, University of Leiden, Leiden, the Netherlands, **4** Translational Neurocircuitry, Max Planck Institute for Metabolism Research, Cologne, Germany, **5** Department of Neurology, University Clinics, Cologne, Germany

* Current address: Integrative Model Based Cognitive Neuroscience Research Unit, REC-G Room 3.03, Nieuwe Achtergracht, Amsterdam

* broseisaacs@gmail.com



OPEN ACCESS

Citation: Isaacs B.R, Trutti A.C, Pelzer E, Tittgemeyer M, Temel Y, Forstmann B.U, et al. (2019) Cortico-basal white matter alterations occurring in Parkinson's disease. PLoS ONE 14(8): e0214343. <https://doi.org/10.1371/journal.pone.0214343>

Editor: Allan Siegel, University of Medicine & Dentistry of NJ - New Jersey Medical School, UNITED STATES

Received: March 5, 2019

Accepted: July 17, 2019

Published: August 19, 2019

Copyright: © 2019 Isaacs et al. This is an open access article distributed under the terms of the [Creative Commons Attribution License](https://creativecommons.org/licenses/by/4.0/), which permits unrestricted use, distribution, and reproduction in any medium, provided the original author and source are credited.

Data Availability Statement: There are ethical restrictions on sharing the de-identified dataset, as imposed by the ethical committee; Ethics Review Board of the University Clinics of Cologne (approval number 12-268). Moreover, multiple clinics were involved in the data acquisition, which at the time had different liability for the data protection. However, the data may be shared for purpose of reproducing the reported results if directly requested from the representative of the data protection officer of the Max Planck Society at

Abstract

Magnetic resonance imaging studies typically use standard anatomical atlases for identification and analyses of (patho-)physiological effects on specific brain areas; these atlases often fail to incorporate neuroanatomical alterations that may occur with both age and disease. The present study utilizes Parkinson's disease and age-specific anatomical atlases of the subthalamic nucleus for diffusion tractography, assessing tracts that run between the subthalamic nucleus and *a-priori* defined cortical areas known to be affected by Parkinson's disease. The results show that the strength of white matter fiber tracts appear to remain structurally unaffected by disease. Contrary to that, Fractional Anisotropy values were shown to decrease in Parkinson's disease patients for connections between the subthalamic nucleus and the pars opercularis of the inferior frontal gyrus, anterior cingulate cortex, the dorsolateral prefrontal cortex and the pre-supplementary motor, collectively involved in preparatory motor control, decision making and task monitoring. While the biological underpinnings of fractional anisotropy alterations remain elusive, they may nonetheless be used as an index of Parkinson's disease. Moreover, we find that failing to account for structural changes occurring in the subthalamic nucleus with age and disease reduce the accuracy and influence the results of tractography, highlighting the importance of using appropriate atlases for tractography.

Introduction

The subthalamic nucleus (STN) is a small region located in the basal ganglia (BG) that is integral to a range of motor behaviors and cognitive functions [1]. Abnormal activity of the STN is implicated in a number of neurodegenerative and neurological disorders including Parkinson's disease (PD). Here, increased indirect pathway activity is thought to increase the inhibition of motor plans rather than reducing inhibitory control [2]. Accordingly, the STN is a

the Max Planck Institute of Metabolism Research: Dr Stefan Vollmar, vollmar@sf.mpg.de. However, to provide full disclosure, Dr Vollmar will directly contact Marc Tittgemeyer as the project leader of the institute with regards to informed consent of the participants.

Funding: This research was supported by an ERC grant from the European Research Council (<https://erc.europa.eu/>, B. U. Forstmann, Stg: 313481) and a Vici grant from the Dutch Organization for Scientific Research (<https://www.nwo.nl/en>, B. U. Forstmann, 016.Vici.185.052). The funders had no role in study design, data collection and analysis, decision to publish, or preparation of the manuscript.

Competing interests: The authors have declared that no competing interests exist.

common neurosurgical target for deep brain stimulation (DBS) for PD patients who no longer appropriately respond to pharmacological interventions, where standard targeting is facilitated by the use of MRI and stereotaxic atlases [3].

However, these atlases are often based on a normal population and fail to account for neuroanatomical variability occurring for a variety of reasons, including age and disease [4–9]. It is widely acknowledged that the anatomy of the STN varies substantially across healthy individuals, with *in-vivo* size estimates ranging from 50mm³ to 270mm³ (See [10] and references therein). Additionally, the STN has been shown to move with age, shifting in the lateral direction in the elderly population [11–14] with additional alterations of STN volume and location occurring in PD [15].

Moreover, the STN demonstrates a complex connectivity profile both within the BG and with the rest of the cortex [16–24]. With regards to PD, both the structural and functional connectivity of the STN has been shown to predict the future outcome and relative success of DBS treatment [25]. This is supported by electrophysiological and functional (f)MRI results which show that specific cortico-basal connections are functionally altered in PD [26–28]. Furthermore, the existing variability in the success of DBS suggests the presence of individual differences in the integrity of specific connections between the STN and different cortical regions.

DBS of the STN is however associated with a number of psychiatric side-effects, cognitive, and emotional disturbances [29,30]. One explanation for these side-effects relates to the somatotopic arrangement of functionally dissimilar cortical projections within the STN [31–34]. In DBS, the implanted electrode may directly stimulate, due to suboptimal placement, or spread current to functionally disparate sub-regions of the nucleus which in-turn interfere with the typical connectivity between the STN and limbic or cognitive cortical areas [35,36].

Given the neuroanatomical alterations that occur in the STN due to orthologic aging or PD, it is crucial to investigate whether additional group specific changes extend to their structural connectivity. The current paper first aims to investigate whether there are disease specific alterations in the connectivity of cortical areas to the subthalamic nucleus in PD patients by using group specific atlases of the STN, and second, to assess whether any connectivity measures may be correlated with disease progression. We chose six cortical areas based on their functional involvements in limbic, cognitive, and motor processes, known to be affected in PD [37–41]. Cortical areas consisted of the pars opercularis of the inferior frontal gyrus (Pop), the anterior cingulate cortex (ACC), the dorsolateral prefrontal cortex (DLPFC), primary motor cortex (M1), supplementary motor area (SMA), and pre-supplementary motor area (pre-SMA). Notably, we use these results to highlight the importance of using group specific atlases for STN identification when ultra-high field (UHF) MRI is not available, given the scarcity of UHF MRI sites relative to the number of DBS centers [42–47].

Materials and methods

Subjects

Seventy PD patients and thirty-one age-matched healthy controls participated in the study (Table 1) (see [48] for more details on subject population). Patients were not required to discontinue their medication for the purposes of this study. The gender imbalance in the PD group was due to the fact that PD is 1.5 times more likely to occur in men than in women [49–51]. Disease related variables were obtained from PD patients, which include UPDRS III scores taken both on and off medication, duration of disease in years, and side of symptom onset (left or right), all obtained from an expert neurologist [52]. Disease progression, as a measure of severity, is calculated by dividing each patients UPDRS off III score by the duration of the disease in years [53]. Medication response is calculated by dividing the UPDRS off III score by

Table 1. Descriptive statistics.

Measure	Parkinson's Disease	Healthy Control
Age (years)	62.01(8.62)	61.94(10.21)
Gender	54m/16f	25m/6f
Disease Duration (years)	6.51(4.64)	-
UPDRS III on	14.46(7.03)	-
UPDRS III off	29.84(12.18)	-
Symptom onset (side)	33l/37r	-

The means and standard deviations (S.D) demographic statistics for both the Parkinson's disease and healthy control group. UPDRS: Unified Parkinson's Disease Rating Scale.

<https://doi.org/10.1371/journal.pone.0214343.t001>

the respective UPDRS on [54]. All healthy controls self-reported no history of psychiatric or neurological disease, and PD patients reported no other neurological complaints than PD. The study was approved by the ethical committee of the University Hospital of Cologne, Germany.

MRI acquisition

Whole-brain anatomical T1-weighted and diffusion-weighted images were acquired for each subject with a Siemens 3T Trio scanner (Erlangen, Germany). T1-weighted images were obtained using a 12-channel array head coil with the following parameters: field of view (MDEFT3D: TR = 1930 ms, TI = 650 ms, TE = 5.8 ms, 128 sagittal slices, voxel size = 1 x 1 x 1.25 mm³, flip angle = 18°). dMRI images were obtained via a spin-echo EPI sequence with a 32-channel array head coil (spin echo EPI: TR = 11200 ms, TE = 87ms, 90 axial slices, voxel size = 1.7 mm isotropic, 60 directions isotropically distributed (b-value = 1000 s/mm²). Distortions due to eddy currents and head motion were corrected using FSL (Version 5.0; www.fmrib.ox.ac.uk/fsl) [55]. Additionally, to provide an anatomical reference for motion correction, seven images without diffusion weighting (b0 images) were acquired at the beginning and after each block per ten diffusion-weighted images. The diffusion-weighted images were then registered to these b0 images (see [48] for more details regarding the data acquisition).

Registration

MRI. All registration steps were conducted using both linear and nonlinear functions with FLIRT and FNIRT (as implemented in FSL version 5.0). All registrations were performed on skull stripped and brain extracted images. T1 weighted images were first linearly registered to the MNI152 T1 1mm brain template with a correlation ratio and 12 DOF. An additional nonlinear transform was applied using the FNIRT function with standard settings, including the previously obtained affine transformation matrix. Individual T1-weighted scans in native space were registered to the respective no-diffusion (b0) images with a mutual information cost function and 6 DOF. A standardized midline exclusion mask in MNI152 space was registered to each subjects b0 images through multiple transforms, by combining the transformation matrices outputted via previous registrations. The midline exclusion mask was visually checked and realigned with an additional registration if necessary. Each step during the registration process was visually assessed for misalignments by comparing several landmarks (ventricles, pons, corpus callosum, cortical surface).

Cortical atlases. The six cortical areas were obtained from <http://www.rbmars.dds.nl/CBPatlases.htm>, created with tractography methods, based on both human and non-human primate neuroanatomy [56–58]. The separate cortical masks were extracted from MNI152

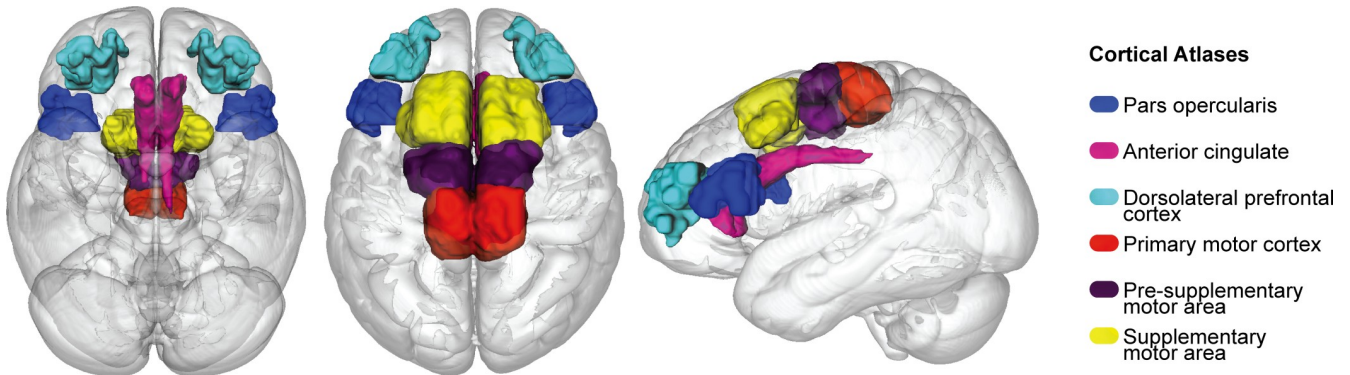


Fig 1. Cortical atlases.

<https://doi.org/10.1371/journal.pone.0214343.g001>

1mm space. The cortical atlases were thresholded at 25% to minimize the occurrence of over estimating the region during registration procedures, which were achieved with a nonlinear transform from MNI152 1mm to individual b0 space using the previously generated transformation matrices from the anatomical registrations, with a nearest neighbor interpolation and 12 DOF (see Fig 1).

Cortical atlases used for probabilistic tractography and the diffusion tensor models in MNI152 1mm space, which consist of the pars opercularis (POp), anterior cingulate cortex (ACC), dorsolateral prefrontal cortex (DLPFC), primary motor cortex (M1), pre supplementary motor area (pre-SMA) and supplementary motor area (SMA).

STN atlases. Group specific PD and elderly probabilistic atlases of the STN were obtained for the respective groups from [59] (Fig 2) (see https://www.nitrc.org/projects/atag_pd/ for probabilistic atlases and ATAG data) and were transformed from MNI152 1mm space to individual b0 space using a nonlinear transform and thresholded by 25%. The non-zero voxel volume in mm³ for each atlas was as follows: PD left = 77; PD right = 70.13; HC left = 164.75; HC right = 138.38 and for the center of gravity (CoG) in MNI152 1mm space: PD left x = -10.44, y = -13.04, z = -8.16; PD right x = 11.84, y = -13.18, z = -89; HC left x = -10.56, y = -13.87, z = -7.10; HC right x = 12.10, y = -12.97, z = -6.20.

Representation of the group specific (left and right) subthalamic nucleus (STN) atlas in MNI152 1mm space where the Parkinson's disease (PD) STN is in purple, and the healthy control (HC) is in orange.



Fig 2. STN atlases.

<https://doi.org/10.1371/journal.pone.0214343.g002>

Probabilistic tractography

Probabilistic tractography was run between *a priori* defined cortical areas and group specific STN's. Diffusion image preprocessing and analyses were achieved using FSL 5.0. The two most likely diffusion directions per voxel were estimated using the bedpostX function as implemented in the FDT toolbox with standard settings [60]. Subsequently, probabilistic tractography (probtrackX) was conducted to calculate continuous structural connections between the respective seed and target region(s). ProbtrackX was run with standard settings (curvature threshold 0.2, 5000 samples, 0.5mm step length, 2000 steps) in each subjects' native diffusion space, separately for left and right hemispheres and aided by the inclusion of a midline exclusion mask.

The term tract strength is used here to index a probability density function, quantifying the ratio of how many streamlines directly and continuously commence from a seed region and terminate at a target area and vice versa (i.e. *seed to target / target to seed*). This density function is a commonly used measure for inferring the strength of structural white matter tracts [60–62]. For more robust measurements, we created an average of each pair of seed-to-target and target-to-seed streamlines [63,64]. To control for spurious tracking, the tracts were thresholded by 10, whereby any voxel containing less than 10 direct samples were excluded from further analyses [64].

We calculated the axial diffusivity (AD), fractional anisotropy (FA), and mean diffusivity (MD) of the seed-to-target and target-to-seed paths derived from the tract strength probability density function approach mentioned in the above section. This was achieved by fitting a voxel wise diffusion tensor model with a weighted least squares regression to each subjects' diffusion image using the DTIFIT function from FDT. Each FDT path was thresholded so that only paths with at least 75 samples were included for further analysis to yield a conservative anatomical representation. Then each pair of corresponding paths were combined (seed-to-target and target-to-seed), binarized and averaged per hemisphere. From these normalized FDT paths we extracted the AD, FA, and MD values per tract, per subject.

Statistical methods

All statistical analyses were conducted within a Bayesian framework (Table 2) using the Bayes-Factor toolbox [65] in R [66], interpreted in light of the assumptions proposed by [67] and

Table 2. Bayes factor interpretation.

Bayes Factor	Interpretation
> 100	Decisive evidence for H1
30–100	Very strong evidence for H1
10–30	Strong evidence for H1
3–10	Substantial evidence for H1
1–3	Anecdotal evidence for H1
1	No evidence
1 / 3–1	Anecdotal evidence for H0
1 / 10–1 / 3	Substantial evidence for H0
1 / 30–1 / 10	Strong evidence for H0
1 / 100–1 / 30	Very strong evidence for H0
< 1 / 100	Decisive evidence for H0

Interpretation of Bayes Factors. H1 refers to the experimental hypothesis, and H0 to the null hypothesis.

<https://doi.org/10.1371/journal.pone.0214343.t002>

adapted by [68]. To test whether there were any group differences in either tract strength or DTI derived metrics [69], we used Bayesian ANOVAs. In this case, structure and tract strength or DTI metric are assessed for main effects and interactions, against the null. This results in four models, assessing for 1. Main effects of structure; 2. Main effects of group; 3. Main effects of both structure and group; and 4. An interaction between structure and group. Both subject and hemisphere were added as random factors, accounting for unequal sample sizes. BFs larger than 100, indexing decisive evidence for the alternative hypothesis, are noted as >100 . All analysis included default prior scales (maximum likelihood) and r-scale prior probabilities.

Our justification for using a Bayesian approach is that we are able to draw inferences on how likely our data is to reflect either the alternative hypothesis (H1) or the null (H0), whereas frequentist approaches using p-values as a significance criterion lead to a dichotomous decision as to whether the data is in support of H1 or H0. Relatedly, Bayesian approaches draw their distribution from the observed data, rather than requiring a Gaussian distribution, which can be difficult to meet with clinical datasets.

Since Bayesian approaches sample from the data itself, the priors for each group are calculated independently, whereby a smaller group will receive greater uncertainty than a larger group for comparison with no trade off with statistical power. Therefore, unequal sample sizes are not thought to negatively impact our results and should not reflect the size of the BFs reported [70,71].

Where multiplicity adjustments are required, prior probabilities will be automatically updated. Generally speaking, the more plausible hypotheses there are, the lower the prior probabilities they will receive. However, Bayesian analyses will automatically prefer the simplest model if it explains the data just as well as a complex model with more parameters. Each test is performed independently of the others so we assume multiple comparisons are not a confounder in the present study[72–75].

To test whether disease progression correlated with either tract strength or the DTI derived metrics, we conducted Bayesian correlation analyses in JASP [73]. Disease progression and medication response were used as separate indices of disease severity [74]. All Bayesian tests used a non-informative prior and a medium sized distribution (conjugate distributions on either side).

Open science

All scripts used to analyse the data can be found at <https://osf.io/4uxxs/>. The data is available upon request from the data protection officer of the Max Planck Society at the Max Planck Institute of Metabolism Research (representative: Dr Stefan Vollmar, vollmar@sf.mpg.de).

Results

Group differences between HC and PD

Demographics. Two samples Bayesian t-tests were conducted to assess for differences in age and gender across groups. For age, the BF_{10} of 0.23 indicates moderate evidence in favour of the null hypothesis as does a BF_{10} of 0.24 for gender. Therefore, we can assume that there is no difference in gender or age between groups and these variables are not included as covariates for further analyses.

Motion parameters. Additional Bayesian t-tests were conducted to test for differences across groups in each of the directional (x, y, z) translation and rotation parameters, which index how much the subject moves during the MRI. All results were in favour of the null hypothesis (rotation x: $BF_{10} = 0.51$, rotation y: $BF_{10} = 0.33$, $BF_{10} = 0.25$, translation x: $BF_{10} =$

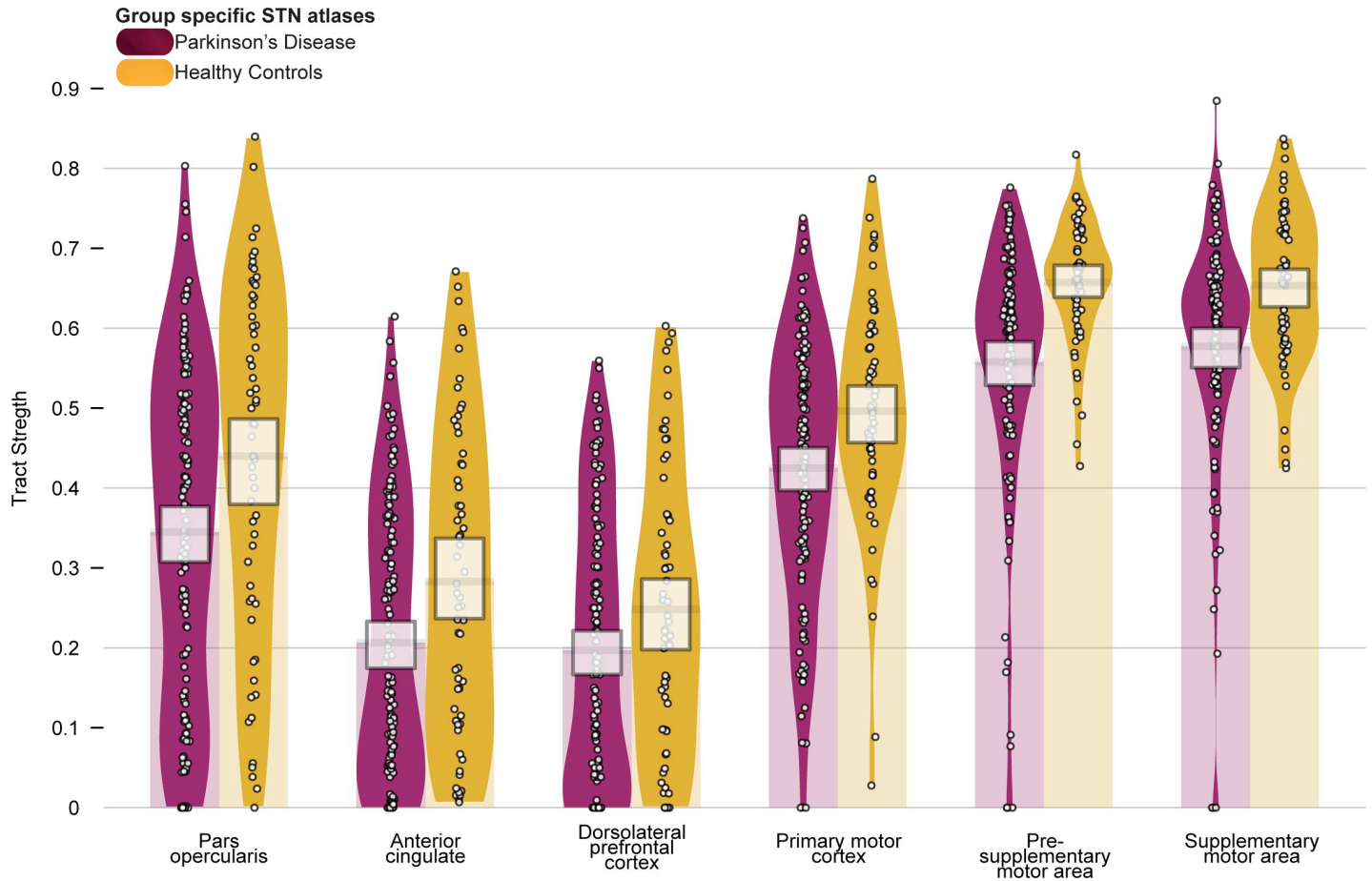


Fig 3. Tract strengths.

<https://doi.org/10.1371/journal.pone.0214343.g003>

0.40, translation y: $BF_{10} = 0.34$, translation z: $BF_{10} = 0.49$). Accordingly, motion parameters are not included as a covariate in further analyses.

Tract strengths. We first set out to test whether there were differences in tract strength between healthy control subjects and PD patients with a mixed effects ANOVA, incorporating subject and hemisphere as random factors (see Fig 3 and Table 3) and run with 50,000

Table 3. Tract strength descriptive statistics per tract, per group.

Tract	Mean (S.D)	
	HC	PD
ACC	0.28 (0.19)	0.21 (0.17)
DLPFC	0.25 (0.18)	0.20 (0.17)
M1	0.50 (0.14)	0.43 (0.16)
Pre-SMA	0.66 (0.08)	0.56 (0.16)
SMA	0.65 (0.09)	0.58 (0.15)
POp	0.44 (0.22)	0.34 (0.21)

The means and standard deviations (S.D) of tract strengths for tracts running between the subthalamic nucleus (STN) and the pars opercularis (POp), anterior cingulate cortex (ACC), dorsolateral prefrontal cortex (DLPFC), primary motor cortex (M1), presupplementary motor area (pre-SMA) and supplementary motor area (SMA), for Parkinson's disease subjects (PD) and healthy controls (HC).

<https://doi.org/10.1371/journal.pone.0214343.t003>

Table 4. Diffusion tensor imaging (DTI) descriptive statistics of axial diffusivity, fractional anisotropy and mean diffusivity per tract, per group.

Tract	Mean (S.D)					
	AD		FA		MD	
	HC	PD	HC	PD	HC	PD
ACC	1.1e-03 (5.1e-05)	1.2e-03 (4.5e-05)	0.40 (0.02)	0.39 (0.03)	8.2e-04 (5.0e-05)	8.1e-04 (5.0e-05)
DLPFC	1.2e-03 (4.7e-05)	1.2e-03 (5.5e-05)	0.37 (0.02)	0.34 (0.02)	8.6e-04 (4.5e-05)	8.6e-04 (5.6e-05)
M1	1.3e-03 (7.7e-05)	1.3e-03 (7.4e-05)	0.42 (0.02)	0.41 (0.04)	8.8e-04 (8.5e-05)	8.8e-04 (8.6e-05)
Pre-SMA	1.2e-0 (5.0e-05)	1.2e-0 (5.0e-05)	0.40 (0.02)	0.39 (0.03)	8.1e-04 (5.2e-05)	8.3e-04 (5.2e-05)
SMA	1.3e-03 (6.6e-05)	1.3e-03 (8.4e-05)	0.39 (0.03)	0.38 (0.03)	9.2e-04 (6.9e-05)	9.3e-04 (9.0e-05)
POp	1.3e-03 (6.6e-05)	1.2e-03 (6.1e-05)	0.36 (0.02)	0.35 (0.02)	9.3e-0 (6.3e-05)	9.4e-04 (5.6e-05)

Mean and standard deviations (S.D) for DTI metrics including axial diffusivity (AD), fractional anisotropy (FA) and mean diffusivity (MD) collapsed across hemisphere per structure (pars opercularis (POp), anterior cingulate cortex (ACC), dorsolateral prefrontal cortex (DLPFC), primary motor cortex (M1), presupplementary motor area (pre-SMA) and supplementary motor area (SMA)) for healthy controls (HC) and Parkinson's disease patients (PD). FA values are marked in bold. There is evidence for group differences for the averaged FA values, which are lower in PD than HC.

<https://doi.org/10.1371/journal.pone.0214343.t004>

iterations. When using group specific atlases of the STN, all models provide decisive evidence for the alternative, against the null (all $BF_{10} = > 100, \pm < 1.45\%$). The largest model included a main effect of group and structure, which is 197 times more likely than the model including an interaction. Therefore we can assume that while tract strengths vary across structure and group, they do not vary within structure across PD and HC, therefore no within group comparisons were conducted.

Tract strengths collapsed across hemisphere per structure (pars opercularis (POp), anterior cingulate cortex (ACC), dorsolateral prefrontal cortex (DLPFC), primary motor cortex (M1), presupplementary motor area (pre-SMA) and supplementary motor area (SMA)), with healthy control (HC) subjects in orange and Parkinson's disease patients (PD) in purple. Tracts are measured from 0 to 1, which is representative of the ratio of the total number of tracts reported between the STN and the given cortical structure (and vice versa). Each point within each element represents a single subject. The width of each element represents the smoothed density. The columns overlapping each bar (each beginning at zero) represent the central tendency, and the bands overlapping each element reflect the 95% highest density intervals, and indicate that the tract strengths for PD are lower than healthy controls across all structures.

DTI metrics: Group differences. To test whether there were group differences in the white matter composition, we extracted the AD, FA, and MD values of the six different tracts. Separate ANOVAs were run to assess AD, FA, and MD across groups (Table 4), also with 50,000 iterations. For AD, the models including a main effect of structure, structure and group, as well as an interaction all provide decisive evidence for the alternative, against the null (all $BF_{10} = > 100, \pm < 1.4\%$). Though the model containing a main effect of only group provides anecdotal evidence for the null ($BF_{10} = 0.36, \pm 1.12\%$). The winning model, including a main effect of only structure was twice as likely than the second winning model, which included main effects of both structure and group. However, according to the interpretation, there is only anecdotal evidence for a difference between these models. Though the main effect of structure is decisively more likely by a BF_{10} of 283 than the model including an interaction. Therefore we can assume that while AD varies across structure and group, it does not vary within structure across PD and HC, therefore no within group comparisons were conducted.

MD models showed the same trend as the AD, whereby a main effect of structure, structure and group, as well as an interaction all provide decisive evidence for the alternative, against the null (all $BF_{10} = > 100, \pm < 2\%$). Though the model containing a main effect of only group

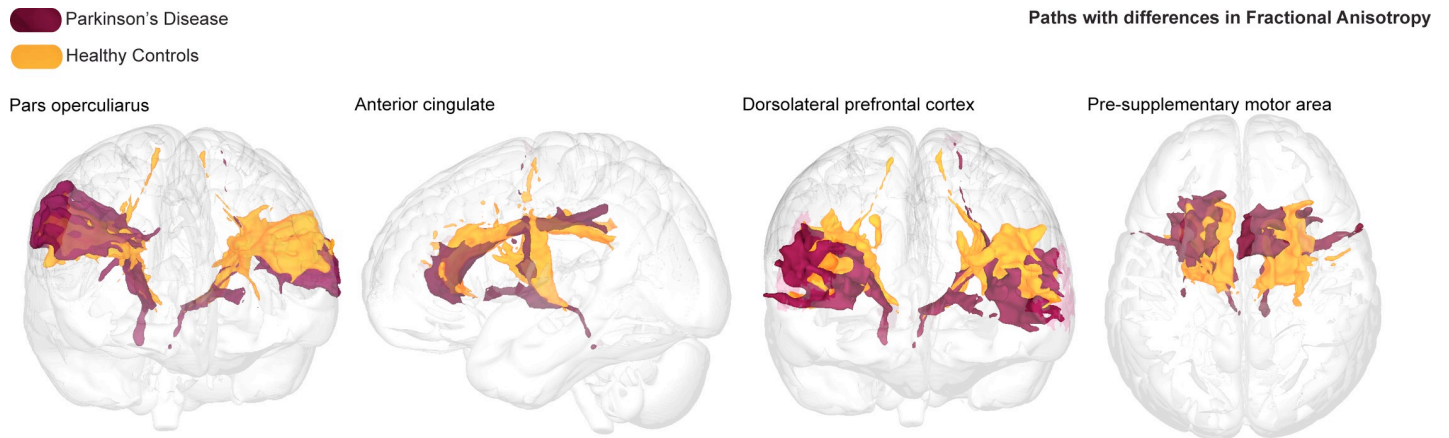


Fig 4. Fractional anisotropy pathways.

<https://doi.org/10.1371/journal.pone.0214343.g004>

provides moderate evidence for the null ($BF_{10} = 0.14, \pm 1.37\%$). The winning model, including a main effect of only structure is five times more likely than the second winning model, which included main effects of both structure and group. According to the interpretation, this is moderate evidence that the main effect of structure wins over a main effect of structure and group. Moreover, the main effect of structure is decisively more likely than the interaction by a BF_{10} of 167.

When assessing FA, all models provide decisive evidence for the alternative, against the null (all $BF_{10} = > 100, \pm < 2.9\%$). The winning model includes the interaction term, and is four times more likely than the second winning model which includes a main effect of structure group, and is decisively more likely than the model including only a main effect of structure by a BF_{10} of 833. Post-hoc Bayesian t-tests were run to assess for the evidence that structure by group differences was greater than zero. Here we find strong evidence for differences between groups for FA values between STN and POP by a BF_{10} of 18.53, with higher FA values for healthy controls than PD patients. Substantial evidence was found for FA values differing across groups between the STN and the ACC ($BF_{10} = 3.05$), which are also higher in healthy controls than PD patients. Decisive evidence was found for the DLPFC ($BF_{10} = 5.31e+10$) and pre-SMA ($BF_{10} = 68.31$) connectivity profiles, again both with higher FA values for healthy controls than PD patients (Fig 4). Anecdotal evidence was found for lower FA for the SMA connectivity profiles in PD than HC ($BF_{10} = 2.35$).

Averaged and thresholded fractional anisotropy (FA) tracts per group running between the subthalamic nucleus (STN) to the pars opercularis (POP), anterior cingulate cortex (ACC), dorsolateral prefrontal cortex (DLPFC), and pre supplementary motor area (pre-SMA), with Parkinson's disease (PD) tracts in purple and healthy control (HC) tracts in orange. In all tracts, the FA was lower for PD compared to healthy controls.

Correlations. Bayesian paired correlations with a Pearson's Rho correlation coefficient was conducted to assess whether for each PD patient, disease progression or medication response correlated with either their tract strength or respective FA measures [73]. Additionally, because the motor related symptoms of PD often begin and continue to exhibit asymmetrically, the side in which symptom onset was first identified (i.e., left or right side of the body) was counterbalanced across hemisphere [76–78]. Symptom onset initiating on the left side of the body was paired with tract strength or FA values arising from the right hemisphere and vice versa for the left hemisphere (contralateral), and a separate correlation test was conducted for those tracts that occur in the hemisphere on the same side as symptom onset (ipsilateral).

This was done in order to control for the lateralization effects of both symptom presentation and brain connectivity and to test whether tract strengths can act as an index of symptom severity.

For disease progression with tract strength, all results reported substantial evidence for no correlation between tract strengths and disease progression. For medication response with tract strength, all results reported anecdotal (ACC) or substantial (DLPFC, M1, pre-SMA, SMA, POP) evidence for no correlation between tract strengths and medication response. For disease progression with averaged FA, the only a tract to show strong evidence of a correlation with disease progression was the DLPFC ipsilateral score ($r = 0.35$, $BF_{10} = 16.50$), where side of symptom onset and hemisphere were the same. All other results reported either anecdotal or substantial evidence for no correlation between FA and disease progression. For medication response with averaged FA, all results reported substantial evidence for no correlation between FA and medication response. See the [S2 File](#) for the full results of the correlation analysis.

Discussion

The current study assessed the strength and microstructural changes occurring in predefined connectivity profiles between the STN and motor, limbic, and cognitive related cortical areas between PD patients and healthy elderly age-matched controls using group specific atlases of the STN.

PD Disease specific alterations

For all six cortical areas, the mean tract strengths were lower for the PD group, however there was no statistical evidence to support substantial differences compared to healthy controls. Moreover, none of the tract strengths between the STN and the cortical areas correlated with measures of disease progression or medication response. It therefore appears unlikely that the strength of any of the measured tracts may be used as a biomarker for PD.

Diffusion tensor models were applied to draw quantitative measurements of each white matter tract. For the original analysis, we found evidence for a reduction in FA for the STN to POP, ACC, DLPFC, and pre-SMA tracts in PD patients compared to healthy controls. The POP is situated anterior to the premotor cortex and has been implicated in motor inhibition [79] which is referred to as the ability to suspend a premeditated motor response to a stimulus or an ongoing response [80]. It has also been proposed that the POP is the origin of “stop signal” behaviors, whereby the inhibition of a motor response results from direct stimulation of the subthalamic nucleus [81]. Moreover, the primary STN-ACC circuit functions to monitor behaviors that involve conflict and therefore task switching and changing decisions [82–84]. Structural and or functional alterations within the STN-POP and ACC connectivity profiles could reflect the symptomatic profile of PD [85,86].

Relatedly, associated functions of STN-pre-SMA circuit also include response inhibition [87], action choices [88–90], task switching and internally generated movements [91,92], which are shown to be disrupted in PD. Assuming structure both shapes and constrains function [93–95], compromised white matter tracts indexed by increased diffusivity and reduced FA could result in abnormal functioning and lead to clinically overt behaviors [96]. A dysfunctional STN-pre-SMA circuit could result in parkinsonian symptoms including micrographia, dysarthria, bradykinesia and hypokinesia, all of which involve a lack appropriate action selection, timing, and irregular task switching [97–99]. A dysfunctional STN-DLPFC circuit could reflect impaired motor control, PD related cognitive decline, and affective complaints [100–102] as well as being linked to dopaminergic abnormalities [103]. However, while reduced FA in specific STN-cortical circuits could be utilized as a biomarker for PD, it is difficult to infer

the exact biological mechanisms underlying alterations in diffusion metrics relative to disease. FA has been considered as a summary measure of white matter integrity, that is highly sensitive to microstructural changes, but less sensitive to the type of change [104–107], though theoretically, a reduction in FA could be driven by a singular or combination of altered AD, MD, or radial diffusivity.

Moreover, white matter consists not only of axons, but oligodendrocytes, astrocytes and microglia and therefore structural changes can affect any of these properties, each of which is associated with a different function [108,109]. Studies have shown that FA correlates with myelination which is associated with speed conduction, though this is dependent on the formation and remodeling of oligodendrocytes and differentiation of oligodendrocyte precursor cells (OCPs) whose function is to determine the production, length and thickness of internodes and therefore also likely to contribute to the FA signal [110–113]. Fewer studies have assessed diffusion parameters in relation to astrocytes, though their contribution to FA signals is likely to be significant given their large occupying volume within both grey and white matter [112,114].

Physiologically, a disruption or structural abnormality occurring anywhere along the axon, for example due to changes in myelination, impaired astrocyte propagation or suboptimal OCP proliferation and differentiation, would impede the rate of conduction and transmission between structures and consequently result in functional impairments [115]. Additionally, more widespread changes in myelin and internode plasticity can be driven by region-specific mechanisms [116,117]. In the case of PD, local signals arising from dopaminergic cell loss with the substantia nigra, or the pathological hyperactivity of the STN could drive the observed structural changes in cortico-basal white matter connections. However, due to the complex timeline and microscopic spatial resolution of these neurochemical and anatomical changes, it is currently not possible to identify which process corresponds with in-vivo human dMRI based FA measures.

Further, diffusivity has been correlated with partial voluming effects arising from free-water [118]. Free-water reflects the presence of water molecules that are not restrained by cellular barriers and therefore do not show a preference for direction, which may be increased in the presence of cellular damage [119]. Thus, the presence of free-water may influence biases on diffusion metrics which can result in a reduction in FA and or an increase in MD [120,121]. For instance, free-water present in diffusion has been shown to reflect FA changes occurring in other PD affected areas such as the substantia nigra [122,123]. Additionally, the measure of tract strength was taken via a probability density function (PDF), which despite being shown as a robust assessment, remains controversial. Measurements indexing relative strength via dynamic causal models, may offer additional information for instance by using tractography data to set priors for connection strengths between regions [124].

Correlates of PD disease severity

Overall, we found no evidence for any correlation between either tract strengths or FA values with disease progression or medication response. With one exception, we found a positive correlation for FA values within the STN-DLPFC connectivity profile increasing with disease progression when the side of symptom onset was matched with hemisphere. An increased FA indicating restricted diffusion along a single direction is not necessarily compatible with explanations of neurodegenerative processes when assuming a higher FA implies increased myelination and axonal density which usually decrease with disease progression. It may be possible that the increased FA is explained by an attempted compensatory, neuroplasticity mechanism and or functional reorganization rather than a direct neurodegenerative process [125,126], or

a response to atypical dopaminergic modulation and levodopa intake [127–129]. Such an adaptive reorganization of structural and functional pathways would, however, occur long before the onset of clinical symptoms, which is not in line with the rather progressed stage of the PD population within this study [76,78]. We therefore remain speculative as to the explanation of this result.

Considerations

The use of MRI poses several challenges when imaging small subcortical nuclei such as the STN [130]. In the current study, the resolution of the anatomical and diffusion sequences was rather large when considering the size of the STN [131]. Imaging the STN is subject to partial voluming effects and blurring of the voxels near the borders of the nucleus, which may contain different tissue types and or fiber bundles of neighboring structures [24,132]. This is further complicated by probabilistic atlases being inherently larger than is often anatomically exact and require registration between template and native space. Such registration procedures employ simple scaling factors that can fail to optimally incorporate morphometric and densitometric variability between individuals [133] which can in turn affect the accuracy of subsequent analysis. We account for this by using group specific atlases, thresholding atlases, and incorporating both rigid and affine transformations during registration procedures. In the [S1 File](#) we included a number of additional analysis to investigate the effects of atlas accuracy.

Manual segmentation of the both the STN and cortical areas for all individuals would be the golden standard, however, the data in the current study did not allow for manual parcellation of the STN or of structurally distinct cortical areas [134,135]. Relatedly, the visualization of the STN would benefit from the use of sub-millimeter resolution imaging with UHF MRI and/or susceptibility-based contrasts [13,136].

Lastly, we do not assess for gender differences. While sexual dimorphisms in PD have been reported [50,99,137,138], it remains controversial as to how sensitive standardized scores such as the UPDRS are at identifying gender differences [137,139]. In addition, we include a relatively small sample size with an unbalanced male to female ratio.

Conclusions and future directions

To conclude, the strength of white matter tracts within the hyper-direct pathway appear unaffected by the pathophysiology of PD. However, decreased FA values of the STN-POP, STN-DLPFC and STN-pre-SMA tracts may be used as a biomarker for disease, though the exact biological mechanisms driving these disease specific alterations in FA remain elusive. Regardless, the differences we find are in the connections to cortical areas involved in preparatory motor control, task monitoring and decision making, rather than cortical areas governing motor output. Further, the results indicate that it is recommended to use an atlas that accounts for anatomical changes associated with PD rather than only age matched controls. See the [S1 File](#) for a control analysis to support the use of group specific atlases. Future work should focus on the use of higher field strengths, alternative tractography methods and harmonization of techniques used to investigate PD [140,141]. Until then, we show that using atlases that are specific to your population can aid analysis where UHF MRI and or manual segmentations are not possible.

Tractography methods hold great promise for their contribution to identification of disease, differential diagnoses between subtypes of parkinsonian syndromes and the application of DBS [142,143]. Such applications require assessment of the biological foundations of diffusion metrics and neuroanatomical factors with specific subsets of disease scales used to evaluate presence and severity.

Supporting information

S1 File. Control analysis. Fig A. STN Atlases. Subthalamic nucleus (STN) atlas in MNI152 1mm space where the Parkinson's disease (PD) STN is in purple, and the healthy control (HC) in orange. The first control analysis is shown where the group specific atlases were switched so that the PD STN was registered to each HC, and vice versa. The last image shows the second control analysis where spheres were derived from the group specific center of gravity coordinates and expanded by 4.5mm. Table A. Tract strength descriptive per tract, per group, for the first control analysis which switches group specific atlases. Fig B. Tract Strengths: First Control Analysis. Tract strengths for the first control analysis, collapsed across hemisphere per structure, with healthy control (HC) subjects in orange and Parkinson's disease (PD) patients in purple. Table B. Tract strength descriptive per tract, per group, for the second control analysis which uses spherical ROIs as an atlas. Fig C. Tract Strengths: Second Control Analysis. Tract strengths for the second control analysis, collapsed across hemisphere per structure, with healthy control (HC) subjects in orange and Parkinson's disease (PD) patients in purple. Table C. Diffusion Tensor Imaging (DTI) descriptive statistics of axial diffusivity, fractional anisotropy and mean diffusivity per tract for the first control analysis. Table D. Diffusion Tensor Imaging (DTI) descriptive statistics of axial diffusivity, fractional anisotropy and mean diffusivity per tract, per group for the second control analysis.

(DOCX)

S2 File. Correlation results. Table A. Pearson's Rho. Interpretation of Pearson's Rho Correlation Coefficients[1]. Table B. Correlation between disease progression and tract strength. Table C. Correlation between medication response and tract strength. Table D. Correlation between disease progression and fractional anisotropy. Table E. Correlation between medication response and fractional anisotropy.

(DOCX)

Author Contributions

Conceptualization: Bethany. R. Isaacs, Yasin Temel, Birte. U. Forstmann, Max. C. Keuken.

Data curation: Anne. C. Trutti, Esther Pelzer, Marc Tittgemeyer.

Formal analysis: Bethany. R. Isaacs, Max. C. Keuken.

Funding acquisition: Birte. U. Forstmann.

Investigation: Bethany. R. Isaacs, Birte. U. Forstmann, Max. C. Keuken.

Methodology: Bethany. R. Isaacs, Anne. C. Trutti, Esther Pelzer, Marc Tittgemeyer, Birte. U. Forstmann, Max. C. Keuken.

Project administration: Birte. U. Forstmann.

Resources: Bethany. R. Isaacs, Anne. C. Trutti, Esther Pelzer, Marc Tittgemeyer, Birte. U. Forstmann, Max. C. Keuken.

Software: Bethany. R. Isaacs, Max. C. Keuken.

Supervision: Yasin Temel, Birte. U. Forstmann, Max. C. Keuken.

Validation: Bethany. R. Isaacs, Esther Pelzer, Marc Tittgemeyer, Max. C. Keuken.

Visualization: Bethany. R. Isaacs.

Writing – original draft: Bethany. R. Isaacs.

Writing – review & editing: Bethany. R. Isaacs, Anne. C. Trutti, Esther Pelzer, Marc Tittgmeier, Yasin Temel, Birte. U. Forstmann, Max. C. Keuken.

References

1. Parent A, Hazrati LN. Functional anatomy of the basal ganglia. II. The place of subthalamic nucleus and external pallidum in basal ganglia circuitry. *Brain Res Brain Res Rev* [Internet]. 1995 Jan [cited 2017 Oct 4]; 20(1):128–54. Available from: <http://www.ncbi.nlm.nih.gov/pubmed/7711765> PMID: 7711765
2. Obeso JA, Rodriguez-Oroz M, Rodriguez M, Lanciego JL, Artieda J, Gonzalo N, et al. Pathophysiology of the basal ganglia in Parkinson's disease. *Trends Neurosci*. 2000; 23(8–19).
3. Perlmutter JS, Mink JW. DEEP BRAIN STIMULATION. *Annu Rev Neurosci* [Internet]. 2006 Jul 21 [cited 2017 Oct 19]; 29(1):229–57. Available from: <http://www.ncbi.nlm.nih.gov/pubmed/16776585>
4. Dickie DA, Shenkin SD, Anblagan D, Lee J, Blesa Cabez M, Rodriguez D, Boardman JP, Waldman A, Job DE, Wardlaw JM. Whole brain magnetic resonance image atlases: a systematic review of existing atlases and caveats for use in population imaging. *Frontiers in neuroinformatics*. 2017 Jan 19; 11:1. <https://doi.org/10.3389/fninf.2017.00001> PMID: 28154532
5. Evans. Brain templates and atlases. *Neuroimage* [Internet]. 2012 Aug 15 [cited 2017 Oct 4]; 62(2):911–22. Available from: <http://www.sciencedirect.com/science/article/pii/S1053811912000419> <https://doi.org/10.1016/j.neuroimage.2012.01.024> PMID: 22248580
6. Lucerna S, Salpietro FM, Alafaci C, Tomasello F. The Reference System: The ca-cp Plane. In: *In Vivo Atlas of Deep Brain Structures* [Internet]. Berlin, Heidelberg: Springer Berlin Heidelberg; 2002 [cited 2017 Oct 4]. p. 1–1. Available from: http://link.springer.com/10.1007/978-3-642-56381-2_1
7. Nakano N, Taneda M, Watanabe A, Kato A. Computed three-dimensional atlas of subthalamic nucleus and its adjacent structures for deep brain stimulation in Parkinson's disease. *ISRN neurology*. 2012 Jan 12;2012.
8. Richter EO, Hoque T, Halliday W, Lozano AM, Saint-Cyr JA. Determining the position and size of the subthalamic nucleus based on magnetic resonance imaging results in patients with advanced Parkinson disease. *J Neurosurg* [Internet]. 2004 Mar [cited 2017 Oct 19]; 100(3):541–6. Available from: <http://www.ncbi.nlm.nih.gov/pubmed/15035292> <https://doi.org/10.3171/jns.2004.100.3.0541> PMID: 15035292
9. Xiao Y, Jannin P, d'Albis T, Guizard N, Haegelen C, Lalys F, Vérin M, Collins DL. Investigation of morphometric variability of subthalamic nucleus, red nucleus, and substantia nigra in advanced Parkinson's disease patients using automatic segmentation and PCA-based analysis. *Human brain mapping*. 2014 Sep; 35(9):4330–44. <https://doi.org/10.1002/hbm.22478> PMID: 24652699
10. Zwirner J, Möbius D, Bechmann I, Arendt T, Hoffmann KT, Jäger C, Lobsien D, Möbius R, Planitz U, Winkler D, Morawski M. Subthalamic nucleus volumes are highly consistent but decrease age-dependently—a combined magnetic resonance imaging and stereology approach in humans. *Human brain mapping*. 2017 Feb; 38(2):909–22. <https://doi.org/10.1002/hbm.23427> PMID: 27726278
11. den Dunnen WFA, Staal MJ. Anatomical alterations of the subthalamic nucleus in relation to age: A postmortem study. *Mov Disord* [Internet]. 2005 Jul 1 [cited 2017 Oct 4]; 20(7):893–8. Available from: <https://doi.org/10.1002/mds.20417> PMID: 15809991
12. Alkemade A, De Hollander G, Keuken MC, Schäfer A, Ott DVM, Schwarz J, et al. Comparison of T2*-weighted and QSM contrasts in Parkinson's disease to visualize the STN with MRI. *PLoS One*. 2017;
13. Keuken MC, Bazin PL, Backhouse K, Beekhuizen S, Himmer L, Kandola A, Lafeber JJ, Prochazkova L, Trutti A, Schäfer A, Turner R. Effects of aging on T_1 , T_2^* , and QSM MRI values in the subcortex. *Brain Structure and Function*. 2017 Aug 1; 222(6):2487–505. <https://doi.org/10.1007/s00429-016-1352-4> PMID: 28168364
14. Kitajima M, Korogi Y, Kakeda S, Moriya J, Ohnari N, Sato T, et al. Human subthalamic nucleus: evaluation with high-resolution MR imaging at 3.0 T. *Neuroradiology* [Internet]. 2008 Aug 29 [cited 2017 Oct 4]; 50(8):675–81. Available from: <http://www.ncbi.nlm.nih.gov/pubmed/18443775> <https://doi.org/10.1007/s00234-008-0388-4> PMID: 18443775
15. Pereira JL, Furie S, Sharim J, Yazdi D, DeSalles AA, Pouratian N. Lateralization of the subthalamic nucleus with age in Parkinson's disease. *Basal ganglia*. 2016 Apr 1; 6(2):83–8. <https://doi.org/10.1016/j.baga.2016.01.003> PMID: 26900546
16. Baudrexel S, Witte T, Seifried C, von Wegner F, Beissner F, Klein JC, Steinmetz H, Deichmann R, Roeper J, Hilker R. Resting state fMRI reveals increased subthalamic nucleus–motor cortex connectivity in Parkinson's disease. *Neuroimage*. 2011 Apr 15; 55(4):1728–38. <https://doi.org/10.1016/j.neuroimage.2011.01.017> PMID: 21255661

17. Brunenberg EJ, Moeskops P, Backes WH, Pollo C, Cammoun L, Vilanova A, Janssen ML, Visser-Vandewalle VE, ter Haar Romeny BM, Thiran JP, Platel B. Structural and resting state functional connectivity of the subthalamic nucleus: identification of motor STN parts and the hyperdirect pathway. *PLoS one*. 2012 Jun 29; 7(6):e39061. <https://doi.org/10.1371/journal.pone.0039061> PMID: 22768059
18. Dyrby TB, Søgaard L V., Parker GJ, Alexander DC, Lind NM, Baaré WFC, et al. Validation of in vitro probabilistic tractography. *Neuroimage* [Internet]. 2007 Oct 1 [cited 2017 Oct 4]; 37(4):1267–77. Available from: <http://www.ncbi.nlm.nih.gov/pubmed/17706434> <https://doi.org/10.1016/j.neuroimage.2007.06.022> PMID: 17706434
19. Jahanshahi M, Obeso I, Rothwell JC, Obeso JA. A fronto-striato-subthalamic-pallidal network for goal-directed and habitual inhibition [Internet]. Vol. 16, *Nature Reviews Neuroscience*. 2015 [cited 2017 Oct 19]. p. 719–32. Available from: <http://www.ncbi.nlm.nih.gov/pubmed/26530468> <https://doi.org/10.1038/nrn4038> PMID: 26530468
20. Lambert C, Zrinzo L, Nagy Z, Lutti A, Hariz M, Foltynie T, et al. Confirmation of functional zones within the human subthalamic nucleus: Patterns of connectivity and sub-parcellation using diffusion weighted imaging. *Neuroimage* [Internet]. 2012 Mar [cited 2017 Oct 4]; 60(1):83–94. Available from: <http://www.ncbi.nlm.nih.gov/pubmed/22173294> <https://doi.org/10.1016/j.neuroimage.2011.11.082> PMID: 22173294
21. Lenglet C, Abosch A, Yacoub E, De Martino F, Sapiro G, Harel N. Comprehensive in vivo mapping of the human basal ganglia and thalamic connectome in individuals using 7T MRI. *PLoS one*. 2012 Jan 3; 7(1):e29153. <https://doi.org/10.1371/journal.pone.0029153> PMID: 22235267
22. Nambu A. Seven problems on the basal ganglia. *Current Opinion in Neurobiology*. 2008.
23. Plantinga BR, Temel Y, Duchin Y, Uludağ K, Patriat R, Roebroek A, et al. Individualized parcellation of the subthalamic nucleus in patients with Parkinson's disease with 7T MRI. *Neuroimage* [Internet]. 2016 Sep 26 [cited 2017 Oct 19]; Available from: <http://www.ncbi.nlm.nih.gov/pubmed/27688203>
24. Plantinga BR, Roebroek A, Kemper VG, Uludağ K, Melse M, Mai J, Kuijf ML, Herrler A, Jahanshahi A, ter Haar Romeny BM, Temel Y. Ultra-high field MRI post mortem structural connectivity of the human subthalamic nucleus, substantia nigra, and globus pallidus. *Frontiers in neuroanatomy*. 2016 Jun 16; 10:66 <https://doi.org/10.3389/fnana.2016.00066> PMID: 27378864
25. Horn A, Reich M, Vorwerk J, Li N, Wenzel G, Fang Q, et al. Connectivity Predicts deep brain stimulation outcome in Parkinson disease. *Ann Neurol* [Internet]. 2017 Jul 1 [cited 2017 Oct 4]; 82(1):67–78. Available from: <https://doi.org/10.1002/ana.24974> PMID: 28586141
26. Litvak V, Jha A, Eusebio A, Oostenveld R, Foltynie T, Limousin P, et al. Resting oscillatory cortico-subthalamic connectivity in patients with Parkinson's disease. *Brain*. 2011; 134(2):359–74.
27. Rowe J, Stephan KE, Friston K, Frackowiak R, Lees A, Passingham R. Attention to action in Parkinson's disease: impaired effective connectivity among frontal cortical regions. *Brain* [Internet]. 2002 Feb [cited 2017 Oct 4]; 125(Pt 2):276–89. Available from: <http://www.ncbi.nlm.nih.gov/pubmed/11844728>
28. Wu T, Wang L, Chen Y, Zhao C, Li K, Chan P. Changes of functional connectivity of the motor network in the resting state in Parkinson's disease. *Neurosci Lett* [Internet]. 2009 Aug 21 [cited 2017 Oct 4]; 460(1):6–10. Available from: <http://www.ncbi.nlm.nih.gov/pubmed/19463891> <https://doi.org/10.1016/j.neulet.2009.05.046> PMID: 19463891
29. Benabid AL, Chabardes S, Mitrofanis J, Pollak P. Deep brain stimulation of the subthalamic nucleus for the treatment of Parkinson's disease. *Lancet Neurol* [Internet]. 2009 Jan [cited 2017 Oct 19]; 8(1):67–81. Available from: <http://www.ncbi.nlm.nih.gov/pubmed/19081516> [https://doi.org/10.1016/S1474-4422\(08\)70291-6](https://doi.org/10.1016/S1474-4422(08)70291-6) PMID: 19081516
30. Wichmann T, DeLong MR. Deep Brain Stimulation for Neurologic and Neuropsychiatric Disorders. *Neuron* [Internet]. 2006 Oct 5 [cited 2017 Oct 19]; 52(1):197–204. Available from: <http://www.ncbi.nlm.nih.gov/pubmed/17015236> <https://doi.org/10.1016/j.neuron.2006.09.022> PMID: 17015236
31. Joel D, Weiner I. The connections of the primate subthalamic nucleus: Indirect pathways and the open-interconnected scheme of basal ganglia-thalamocortical circuitry. *Brain Research Reviews*. 1997.
32. Miyachi S, Lu X, Imanishi M, Sawada K, Nambu A, Takada M. Somatotopically arranged inputs from putamen and subthalamic nucleus to primary motor cortex. *Neurosci Res* [Internet]. 2006 Nov [cited 2017 Oct 19]; 56(3):300–8. Available from: <http://www.ncbi.nlm.nih.gov/pubmed/16973231> <https://doi.org/10.1016/j.neures.2006.07.012> PMID: 16973231
33. Nambu A, Takada M, Inase M, Tokuno H. Dual somatotopical representations in the primate subthalamic nucleus: evidence for ordered but reversed body-map transformations from the primary motor cortex and the supplementary motor area. *J Neurosci* [Internet]. 1996 Apr 15 [cited 2017 Oct 19]; 16(8):2671–83. Available from: <http://www.ncbi.nlm.nih.gov/pubmed/8786443> PMID: 8786443

34. Romanelli P, Esposito V, Schaal DW, Heit G. Somatotopy in the basal ganglia: experimental and clinical evidence for segregated sensorimotor channels. *Brain Res Rev* [Internet]. 2005 Feb [cited 2017 Oct 19]; 48(1):112–28. Available from: <http://linkinghub.elsevier.com/retrieve/pii/S0165017304001250> <https://doi.org/10.1016/j.brainresrev.2004.09.008> PMID: 15708631
35. Saint-Cyr JA, Hoque T, Pereira LC, Dostrovsky JO, Hutchison WD, Mikulis DJ, Abosch A, Sime E, Lang AE, Lozano AM. Localization of clinically effective stimulating electrodes in the human subthalamic nucleus on magnetic resonance imaging. *Journal of neurosurgery*. 2002 Nov 1; 97(5):1152–66. <https://doi.org/10.3171/jns.2002.97.5.1152> PMID: 12450038
36. Temel Y, Blokland A, Steinbusch HW, Visser-Vandewalle V. The functional role of the subthalamic nucleus in cognitive and limbic circuits. *Progress in neurobiology*. 2005 Aug 1; 76(6):393–413. <https://doi.org/10.1016/j.pneurobio.2005.09.005> PMID: 16249050
37. Hu Y, Dolcos S. Trait anxiety mediates the link between inferior frontal cortex volume and negative affective bias in healthy adults. *Social cognitive and affective neuroscience*. 2017 Mar 1; 12(5):775–82. <https://doi.org/10.1093/scan/nsx008> PMID: 28158829
38. Kane MJ, Engle RW. The role of prefrontal cortex in working-memory capacity, executive attention, and general fluid intelligence: An individual-differences perspective. *Psychonomic bulletin & review*. 2002 Dec 1; 9(4):637–71.
39. Nambu A, Tokuno H, Takada M. Functional significance of the cortico-subthalamo-pallidal “hyperdirect” pathway. *Neurosci Res* [Internet]. 2002 Jun [cited 2017 Oct 19]; 43(2):111–7. Available from: <http://www.ncbi.nlm.nih.gov/pubmed/12067746> PMID: 12067746
40. MacDonald AW, Cohen JD, Stenger VA, Carter CS. Dissociating the role of the dorsolateral prefrontal and anterior cingulate cortex in cognitive control. *Science*. 2000 Jun 9; 288(5472):1835–8. <https://doi.org/10.1126/science.288.5472.1835> PMID: 10846167
41. Molnar-Szakacs I, Iacoboni M, Koski L, Mazziotta JC. Functional segregation within pars opercularis of the inferior frontal gyrus: evidence from fMRI studies of imitation and action observation. *Cerebral Cortex*. 2004 Oct 28; 15(7):986–94. <https://doi.org/10.1093/cercor/bhh199> PMID: 15513929
42. Abosch A, Yacoub E, Ugurbil K, Harel N. An assessment of current brain targets for deep brain stimulation surgery with susceptibility-weighted imaging at 7 tesla. *Neurosurgery*. 2010 Dec 1; 67(6):1745–56 <https://doi.org/10.1227/NEU.0b013e3181f74105> PMID: 21107206
43. Beisteiner R, Robinson S, Wurnig M, Hilbert M, Merksa K, Rath J, Höllinger I, Klinger N, Marosi C, Trattng S, Geißler A. Clinical fMRI: evidence for a 7 T benefit over 3 T. *Neuroimage*. 2011 Aug 1; 57(3):1015–21. <https://doi.org/10.1016/j.neuroimage.2011.05.010> PMID: 21620980
44. Cho ZH, Min HK, Oh SH, Han JY, Park CW, Chi JG, Kim YB, Paek SH, Lozano AM, Lee KH. Direct visualization of deep brain stimulation targets in Parkinson disease with the use of 7-tesla magnetic resonance imaging. *Journal of neurosurgery*. 2010 Sep 1; 113(3):639–47. <https://doi.org/10.3171/2010.3.JNS091385> PMID: 20380532
45. Cho ZH, Kim YB, Han JY, Min HK, Kim KN, Choi SH, Veklerov E, Shepp LA. New brain atlas—mapping the human brain in vivo with 7.0 T MRI and comparison with postmortem histology: will these images change modern medicine?. *International Journal of Imaging Systems and Technology*. 2008; 18(1): 2–8.
46. Forstmann BU, Keuken MC, Jahfari S, Bazin PL, Neumann J, Schäfer A, et al. Cortico-subthalamic white matter tract strength predicts interindividual efficacy in stopping a motor response. *Neuroimage* [Internet]. 2012; 60(1):370–5. Available from: <http://dx.doi.org/10.1016/j.neuroimage.2011.12.044>
47. Hoffmann AL, Mottaghy FM, Janssen F, Peerlings J, Compter I, Wiggins CJ, et al. Characterizing geometrical accuracy in clinically optimised 7T and 3T magnetic resonance images for high-precision radiation treatment of brain tumours. *Phys Imaging Radiat Oncol* [Internet]. 2019; 9(November 2018):35–42. Available from: <https://linkinghub.elsevier.com/retrieve/pii/S2405631618300447>
48. Feis DL, Pelzer EA, Timmermann L, Tittgemeyer M. Classification of symptom-side predominance in idiopathic Parkinson's disease. *NPJ Parkinson's disease*. 2015 Oct 29; 1:15018. <https://doi.org/10.1038/npparkd.2015.18> PMID: 28725686
49. Marceglia SA, Mrakic-Sposta S, Foffani G, Cogiamanian F, Caputo E, Egidi M, Barbieri S, Priori A. Gender-related differences in the human subthalamic area: a local field potential study. *European Journal of Neuroscience*. 2006 Dec; 24(11):3213–22. <https://doi.org/10.1111/j.1460-9568.2006.05208.x> PMID: 17156382
50. Miller IN, Cronin-Golomb A. Gender differences in Parkinson's disease: clinical characteristics and cognition. *Movement Disorders*. 2010 Dec 15; 25(16):2695–703. <https://doi.org/10.1002/mds.23388> PMID: 20925068
51. Moisan F, Kab S, Mohamed F, Canonico M, Le Guern M, Quintin C, Carcaillon L, Nicolau J, Duport N, Singh-Manoux A, Boussac-Zarebska M. Parkinson disease male-to-female ratios increase with age:

- French nationwide study and meta-analysis. *J Neurol Neurosurg Psychiatry*. 2016 Sep 1; 87(9):952–7. <https://doi.org/10.1136/jnnp-2015-312283> PMID: 26701996
52. Tomer R, Levin BE, Weiner WJ. Side of onset of motor symptoms influences cognition in Parkinson's disease. *Annals of Neurology: Official Journal of the American Neurological Association and the Child Neurology Society*. 1993 Oct; 34(4):579–84.
 53. Baumann CR, Held U, Valko PO, Wienecke M, Waldvogel D. Body side and predominant motor features at the onset of Parkinson's disease are linked to motor and nonmotor progression. *Movement Disorders*. 2014 Feb; 29(2):207–13. <https://doi.org/10.1002/mds.25650> PMID: 24105646
 54. Bordelon YM, Hays RD, Vassar SD, Diaz N, Bronstein J, Vickrey BG. Medication responsiveness of motor symptoms in a population-based study of parkinson disease. *Parkinsons Dis*. 2011; 2011.
 55. Jenkinson M, Beckmann CF, Behrens TE, Woolrich MW, Smith SM. FSL 1. *Neuroimage*. 2012.
 56. Neubert F-X, Mars RB, Thomas AG, Sallet J, Rushworth MFS. Comparison of human ventral frontal cortex areas for cognitive control and language with areas in monkey frontal cortex. *Neuron* [Internet]. 2014 Feb 5 [cited 2017 Oct 19]; 81(3):700–13. Available from: <http://www.ncbi.nlm.nih.gov/pubmed/24485097> <https://doi.org/10.1016/j.neuron.2013.11.012> PMID: 24485097
 57. Sallet J, Mars RB, Noonan MP, Neubert F-X, Jbabdi S, O'Reilly JX, et al. The Organization of Dorsal Frontal Cortex in Humans and Macaques. *J Neurosci* [Internet]. 2013 Jul 24 [cited 2017 Oct 19]; 33(30):12255–74. Available from: <http://www.ncbi.nlm.nih.gov/pubmed/23884933> <https://doi.org/10.1523/JNEUROSCI.5108-12.2013> PMID: 23884933
 58. Neubert FX, Mars RB, Sallet J, Rushworth MF. Connectivity reveals relationship of brain areas for reward-guided learning and decision making in human and monkey frontal cortex. *Proceedings of the national academy of sciences*. 2015 May 19; 112(20):E2695–704.
 59. Alkemade A, de Hollander G, Keuken MC, Schäfer A, Ott DVM, Schwarz J, et al. Comparison of T2*-weighted and QSM contrasts in Parkinson's disease to visualize the STN with MRI. Jiang Q, editor. *PLoS One* [Internet]. 2017 Apr 19 [cited 2017 Oct 19]; 12(4):e0176130. Available from: <https://doi.org/10.1371/journal.pone.0176130> PMID: 28423027
 60. Behrens TE, Berg HJ, Jbabdi S, Rushworth MF, Woolrich MW. Probabilistic diffusion tractography with multiple fibre orientations: What can we gain?. *Neuroimage*. 2007 Jan 1; 34(1):144–55. <https://doi.org/10.1016/j.neuroimage.2006.09.018> PMID: 17070705
 61. Khalsa S, Mayhew SD, Chechlacz M, Bagary M, Bagshaw AP. The structural and functional connectivity of the posterior cingulate cortex: Comparison between deterministic and probabilistic tractography for the investigation of structure–function relationships. *Neuroimage*. 2014 Nov 15; 102:118–27. <https://doi.org/10.1016/j.neuroimage.2013.12.022> PMID: 24365673
 62. van den Bos W, Rodriguez CA, Schweitzer JB, McClure SM. Connectivity strength of dissociable striatal tracts predict individual differences in temporal discounting. *Journal of Neuroscience*. 2014 Jul 30; 34(31):10298–310. <https://doi.org/10.1523/JNEUROSCI.4105-13.2014> PMID: 25080591
 63. Boebel W, Forstmann BU, Keuken MC. A test-retest reliability analysis of diffusion measures of white matter tracts relevant for cognitive control. *Psychophysiology* [Internet]. 2017 Jan 1 [cited 2017 Oct 19]; 54(1):24–33. Available from: <https://doi.org/10.1111/psyp.12769> PMID: 28000260
 64. Forstmann BU, Anwander A, Schäfer A, Neumann J, Brown S, Wagenmakers E-J, et al. Cortico-striatal connections predict control over speed and accuracy in perceptual decision making. *Proc Natl Acad Sci U S A* [Internet]. 2010 Sep 7 [cited 2017 Oct 19]; 107(36):15916–20. Available from: <http://www.ncbi.nlm.nih.gov/pubmed/20733082> <https://doi.org/10.1073/pnas.1004932107> PMID: 20733082
 65. Morey RD, Wagenmakers EJ. Simple relation between Bayesian order-restricted and point-null hypothesis tests. *Statistics & Probability Letters*. 2014 Sep 1; 92:121–4.
 66. R Development Core Team. *R: A Language and Environment for Statistical Computing*. R Found Stat Comput. 2011.
 67. Jeffreys H. *The theory of probability*. Oxford: OUP; 1998.
 68. Wetzels R, Matzke D, Lee MD, Rouder JN, Iverson GJ, Wagenmakers EJ. Statistical evidence in experimental psychology: An empirical comparison using 855 t tests. *Perspectives on Psychological Science*. 2011 May; 6(3):291–8. <https://doi.org/10.1177/1745691611406923> PMID: 26168519
 69. Woolrich MW, Jbabdi S, Patenaude B, Chappell M, Makni S, Behrens T, et al. Bayesian analysis of neuroimaging data in FSL. *Neuroimage* [Internet]. 2009; 45(1 Suppl):S173–86. Available from: <https://doi.org/10.1016/j.neuroimage.2008.10.055> PMID: 19059349
 70. Akaike H. (1998). Likelihood and the Bayes procedure. In *Selected Papers of Hirotugu Akaike* (pp. 309–332). Springer, New York, NY.
 71. Rouder JN, Morey RD, Verhagen J, Swagman AR, Wagenmakers EJ. Bayesian analysis of factorial designs. *Psychol Methods*. 2017; 22(2):304–21. <https://doi.org/10.1037/met0000057> PMID: 27280448

72. Evans NJ, Wagenmakers E-J. Theoretically meaningful models can answer clinically relevant questions. *Brain* [Internet]. 2019; 142(5):1170–2. Available from: <https://academic.oup.com/brain/article/142/5/1170/5481094> <https://doi.org/10.1093/brain/awz096> PMID: 31032845
73. Berry DA, Hochberg Y. Bayesian perspectives on multiple comparisons. *J Stat Plan Inference*. 1999; 82(1–2):215–27.
74. JASP Team. JASP. [Computer software]. 2019.
75. Perlmutter JS. Assessment of Parkinson disease manifestations. *Current protocols in neuroscience*. 2009 Oct; 49(1):10–.
76. Braak H, Bohl JR, Müller CM, Rüb U, de Vos RA, Del Tredici K. Stanley Fahn Lecture 2005: The staging procedure for the inclusion body pathology associated with sporadic Parkinson's disease reconsidered. *Movement disorders: official journal of the Movement Disorder Society*. 2006 Dec; 21(12):2042–51.
77. Hilker R, Schweitzer K, Coburger S, Ghaemi M, Weisenbach S, Jacobs AH, et al. Nonlinear progression of Parkinson disease as determined by serial positron emission tomographic imaging of striatal fluorodopa F 18 activity. *Arch Neurol*. 2005;
78. Sharott A, Gulberti A, Zittel S, Jones AA, Fickel U, Münchau A, Köppen JA, Gerloff C, Westphal M, Buhmann C, Hamel W. Activity parameters of subthalamic nucleus neurons selectively predict motor symptom severity in Parkinson's disease. *Journal of Neuroscience*. 2014 Apr 30; 34(18):6273–85. <https://doi.org/10.1523/JNEUROSCI.1803-13.2014> PMID: 24790198
79. Curley LB, Newman E, Thompson WK, Brown TT, Hagler DJ, Akshoomoff N, Reuter C, Dale AM, Jerinigan TL. Cortical morphology of the pars opercularis and its relationship to motor-inhibitory performance in a longitudinal, developing cohort. *Brain Structure and Function*. 2018 Jan 1; 223(1):211–20. <https://doi.org/10.1007/s00429-017-1480-5> PMID: 28756486
80. Aron AR, Robbins TW, Poldrack RA. Inhibition and the right inferior frontal cortex. *Trends in cognitive sciences*. 2004 Apr 1; 8(4):170–7. <https://doi.org/10.1016/j.tics.2004.02.010> PMID: 15050513
81. Chambers CD, Garavan H, Bellgrove MA. Insights into the neural basis of response inhibition from cognitive and clinical neuroscience. *Neuroscience & biobehavioral reviews*. 2009 May 1; 33(5):631–46.
82. Schroeder U, Kuehler A, Haslinger B, Erhard P, Fogel W, Tronnier VM, Lange KW, Boecker H, Ceballos-Baumann AO. Subthalamic nucleus stimulation affects striato-anterior cingulate cortex circuit in a response conflict task: a PET study. *Brain*. 2002 Sep 1; 125(9):1995–2004.
83. Botvinick MM. Conflict monitoring and decision making: reconciling two perspectives on anterior cingulate function. *Cognitive, Affective, & Behavioral Neuroscience*. 2007 Dec 1; 7(4):356–66.
84. Bryden DW, Brockett AT, Blume E, Heatley K, Zhao A, Roesch MR. Single neurons in anterior cingulate cortex signal the need to change action during performance of a stop-change task that induces response competition. *Cerebral Cortex*. 2018 Feb 3; 29(3):1020–31.
85. Kamagata K, Zalesky A, Hatano T, Di Biase MA, El Samad O, Saiki S, Shimoji K, Kumamaru KK, Kamiya K, Hori M, Hattori N. Connectome analysis with diffusion MRI in idiopathic Parkinson's disease: Evaluation using multi-shell, multi-tissue, constrained spherical deconvolution. *NeuroImage: Clinical*. 2018 Jan 1; 17:518–29.
86. Theilmann RJ, Reed JD, Song DD, Huang MX, Lee RR, Litvan I, Harrington DL. White-matter changes correlate with cognitive functioning in Parkinson's disease. *Frontiers in neurology*. 2013 Apr 12; 4:37. <https://doi.org/10.3389/fneur.2013.00037> PMID: 23630517
87. King AV, Linke J, Gass A, Hennerici MG, Tost H, Poupon C, Wessa M. Microstructure of a three-way anatomical network predicts individual differences in response inhibition: a tractography study. *NeuroImage*. 2012 Jan 16; 59(2):1949–59. <https://doi.org/10.1016/j.neuroimage.2011.09.008> PMID: 21939775
88. Boorman ED, O'Shea J, Sebastian C, Rushworth MFS, Johansen-Berg H. Individual Differences in White-Matter Microstructure Reflect Variation in Functional Connectivity during Choice. *Curr Biol* [Internet]. 2007 Aug 21 [cited 2017 Oct 4]; 17(16):1426–31. Available from: <http://www.ncbi.nlm.nih.gov/pubmed/17689962> <https://doi.org/10.1016/j.cub.2007.07.040> PMID: 17689962
89. Johansen-Berg H. Behavioural relevance of variation in white matter microstructure. *Curr Opin Neuro* [Internet]. 2010 Jun [cited 2017 Oct 19];1. Available from: <http://content.wkhealth.com/linkback/openurl?sid=WKPTLP:landingpage&an=00019052-900000000-99866>
90. Neubert FX, Mars RB, Buch ER, Olivier E, Rushworth MF. Cortical and subcortical interactions during action reprogramming and their related white matter pathways. *Proceedings of the National Academy of Sciences*. 2010 Jul 27; 107(30):13240–5.

91. Gowen E, Miall RC. Differentiation between external and internal cuing: an fMRI study comparing tracing with drawing. *Neuroimage*. 2007 Jun 1; 36(2):396–410. <https://doi.org/10.1016/j.neuroimage.2007.03.005> PMID: 17448689
92. Nachev P, Kennard C, Husain M. Functional role of the supplementary and pre-supplementary motor areas. *Nature Reviews Neuroscience*. 2008 Nov; 9(11):856. <https://doi.org/10.1038/nrn2478> PMID: 18843271
93. Hagmann P, Sporns O, Madan N, Cammoun L, Pienaar R, Wedeen VJ, Meuli R, Thiran JP, Grant PE. White matter maturation reshapes structural connectivity in the late developing human brain. *Proceedings of the National Academy of Sciences*. 2010 Nov 2; 107(44):19067–72.
94. Honey CJ, Sporns O, Cammoun L, Gigandet X, Thiran JP, Meuli R, Hagmann P. Predicting human resting-state functional connectivity from structural connectivity. *Proceedings of the National Academy of Sciences*. 2009 Feb 10; 106(6):2035–40.
95. Honey CJ, Thivierge JP, Sporns O. Can structure predict function in the human brain?. *Neuroimage*. 2010 Sep 1; 52(3):766–76. <https://doi.org/10.1016/j.neuroimage.2010.01.071> PMID: 20116438
96. Tinaz S, Lauro PM, Ghosh P, Lungu C, Horovitz SG. Changes in functional organization and white matter integrity in the connectome in Parkinson's disease. *Neuroimage: Clinical*. 2017 Jan 1; 13:395–404.
97. Artieda J, Pastor MA, Lacruz F, Obeso JA. Temporal discrimination is abnormal in Parkinson's disease. *Brain*. 1992 Feb 1; 115(1):199–210
98. Frank MJ, Samanta J, Moustafa AA, Sherman SJ. Hold your horses: impulsivity, deep brain stimulation, and medication in parkinsonism. *science*. 2007 Nov 23; 318(5854):1309–12. <https://doi.org/10.1126/science.1146157> PMID: 17962524
99. Wylie SA, Ridderinkhof KR, Bashore TR, van den Wildenberg WP. The effect of Parkinson's disease on the dynamics of on-line and proactive cognitive control during action selection. *Journal of cognitive neuroscience*. 2010 Sep; 22(9):2058–73. <https://doi.org/10.1162/jocn.2009.21326> PMID: 19702465
100. Chaudhuri KR, Schapira AH. Non-motor symptoms of Parkinson's disease: dopaminergic pathophysiology and treatment. *The Lancet Neurology*. 2009 May 1; 8(5):464–74. [https://doi.org/10.1016/S1474-4422\(09\)70068-7](https://doi.org/10.1016/S1474-4422(09)70068-7) PMID: 19375664
101. Forsaa EB, Larsen JP, Wentzel-Larsen T, Goetz CG, Stebbins GT, Aarsland D, Alves G. A 12-year population-based study of psychosis in Parkinson disease. *Archives of Neurology*. 2010 Aug 1; 67(8):996–1001. <https://doi.org/10.1001/archneurol.2010.166> PMID: 20697051
102. Santangelo G, Trojano L, Vitale C, Ianniciello M, Amboni M, Grossi D, et al. A neuropsychological longitudinal study in Parkinson's patients with and without hallucinations. *Mov Disord [Internet]*. 2007 Sep 25 [cited 2017 Oct 4]; 22(16):2418–25. Available from: <http://www.ncbi.nlm.nih.gov/pubmed/17894370> <https://doi.org/10.1002/mds.21746> PMID: 17894370
103. Markett S, de Reus MA, Reuter M, Montag C, Weber B, Schoene-Bake JC, van den Heuvel MP. Variation on the dopamine D2 receptor gene (DRD2) is associated with basal ganglia-to-frontal structural connectivity. *Neuroimage*. 2017 Jul 15; 155:473–9. <https://doi.org/10.1016/j.neuroimage.2017.04.005> PMID: 28392487
104. Jones DK, Knösche TR, Turner R. White matter integrity, fiber count, and other fallacies: the do's and don'ts of diffusion MRI. *Neuroimage*. 2013 Jun 1; 73:239–54. <https://doi.org/10.1016/j.neuroimage.2012.06.081> PMID: 22846632
105. Kim HJ, Kim SJ, Kim HS, Choi CG, Kim N, Han S, Jang EH, Chung SJ, Lee CS. Alterations of mean diffusivity in brain white matter and deep gray matter in Parkinson's disease. *Neuroscience letters*. 2013 Aug 29; 550:64–8. <https://doi.org/10.1016/j.neulet.2013.06.050> PMID: 23831353
106. Roberts RE, Anderson EJ, Husain M. White matter microstructure and cognitive function. *Neuroscientist [Internet]*. 2013 Feb [cited 2017 Oct 4]; 19(1):8–15. Available from: <http://www.ncbi.nlm.nih.gov/pubmed/22020545> <https://doi.org/10.1177/1073858411421218> PMID: 22020545
107. Ziegler E, Rouillard M, André E, Coolen T, Stender J, Balteau E, Phillips C, Garraux G. Mapping track density changes in nigrostriatal and extranigral pathways in Parkinson's disease. *Neuroimage*. 2014 Oct 1; 99:498–508. <https://doi.org/10.1016/j.neuroimage.2014.06.033> PMID: 24956065
108. Chong SC, Rosenberg SS, Fancy SP, Zhao C, Shen YA, Hahn AT, McGee AW, Xu X, Zheng B, Zhang LI, Rowitch DH. Neurite outgrowth inhibitor Nogo-A establishes spatial segregation and extent of oligodendrocyte myelination. *Proceedings of the National Academy of Sciences*. 2012 Jan 24; 109(4):1299–304.
109. Chong SYC, Rosenberg SS, Fancy SPJ, Zhao C, Shen Y-AA, Hahn AT, et al. Neurite outgrowth inhibitor Nogo-A establishes spatial segregation and extent of oligodendrocyte myelination. *Proc Natl Acad Sci U S A [Internet]*. 2012 Jan 24 [cited 2019 Feb 22]; 109(4):1299–304. Available from: <http://www.ncbi.nlm.nih.gov/pubmed/22160722> <https://doi.org/10.1073/pnas.1113540109> PMID: 22160722

110. Bechler ME, Swire M, French-Constant C. Intrinsic and adaptive myelination—A sequential mechanism for smart wiring in the brain. *Developmental neurobiology*. 2018 Feb; 78(2):68–79. <https://doi.org/10.1002/dneu.22518> PMID: 28834358
111. Swire M. Seeing Is Believing: Myelin Dynamics in the Adult CNS. *Neuron*. 2018 May 16; 98(4):684–6. <https://doi.org/10.1016/j.neuron.2018.05.005> PMID: 29772200
112. Johansen-Berg H, Baptista CS, Thomas AG. Human structural plasticity at record speed. *Neuron*. 2012 Mar 22; 73(6):1058–60. <https://doi.org/10.1016/j.neuron.2012.03.001> PMID: 22445333
113. Sampaio-Baptista C, Johansen-Berg H. White Matter Plasticity in the Adult Brain. *Neuron* [Internet]. 2017; 96(6):1239–51. Available from: <https://doi.org/10.1016/j.neuron.2017.11.026> PMID: 29268094
114. Walhovd KB, Johansen-Berg H, Karadottir RT. Unraveling the secrets of white matter—bridging the gap between cellular, animal and human imaging studies. *Neuroscience*. 2014 Sep 12; 276:2–13. <https://doi.org/10.1016/j.neuroscience.2014.06.058> PMID: 25003711
115. Fields RD. A new mechanism of nervous system plasticity: activity-dependent myelination. *Nature Reviews Neuroscience*. 2015 Dec; 16(12):756. <https://doi.org/10.1038/nrn4023> PMID: 26585800
116. Auer F, Vagionitis S, Czopka T. Evidence for myelin sheath remodeling in the CNS revealed by in vivo imaging. *Current Biology*. 2018 Feb 19; 28(4):549–59. <https://doi.org/10.1016/j.cub.2018.01.017> PMID: 29429620
117. Mitev S, Gobius I, Fenlon LR, McDougall SJ, Hawkes D, Xing YL, Bujalka H, Gundlach AL, Richards LJ, Kilpatrick TJ, Merson TD. Pharmacogenetic stimulation of neuronal activity increases myelination in an axon-specific manner. *Nature communications*. 2018 Jan 22; 9(1):306. <https://doi.org/10.1038/s41467-017-02719-2> PMID: 29358753
118. Archer DB, Patten C, Coombes SA. Free-water and free-water corrected fractional anisotropy in primary and premotor corticospinal tracts in chronic stroke. *Human brain mapping*. 2017 Sep; 38(9):4546–62. <https://doi.org/10.1002/hbm.23681> PMID: 28590584
119. Planetta PJ, Ofori E, Pasternak O, Burciu RG, Shukla P, DeSimone JC, Okun MS, McFarland NR, Vaillancourt DE. Free-water imaging in Parkinson's disease and atypical parkinsonism. *Brain*. 2015 Dec 23; 139(2):495–508.
120. Metzler-Baddeley C, O'Sullivan MJ, Bells S, Pasternak O, Jones DK. How and how not to correct for CSF-contamination in diffusion MRI. *Neuroimage*. 2012 Jan 16; 59(2):1394–403. <https://doi.org/10.1016/j.neuroimage.2011.08.043> PMID: 21924365
121. Hoy AR, Koay CG, Kecskemeti SR, Alexander AL. Optimization of a free water elimination two-compartment model for diffusion tensor imaging. *Neuroimage*. 2014 Dec 1; 103:323–33. <https://doi.org/10.1016/j.neuroimage.2014.09.053> PMID: 25271843
122. Chung JW, Burciu RG, Ofori E, Shukla P, Okun MS, Hess CW, Vaillancourt DE. Parkinson's disease diffusion MRI is not affected by acute antiparkinsonian medication. *NeuroImage: Clinical*. 2017 Jan 1; 14:417–21.
123. Ofori E, Pasternak O, Planetta PJ, Li H, Burciu RG, Snyder AF, Lai S, Okun MS, Vaillancourt DE. Longitudinal changes in free-water within the substantia nigra of Parkinson's disease. *Brain*. 2015 May 16; 138(8):2322–31.
124. Stephan KE, Tittgemeyer M, Knösche TR, Moran RJ, Friston KJ. Tractography-based priors for dynamic causal models. *Neuroimage*. 2009 Oct 1; 47(4):1628–38. <https://doi.org/10.1016/j.neuroimage.2009.05.096> PMID: 19523523
125. Dayan E, Browner N. Alterations in striato-thalamo-pallidal intrinsic functional connectivity as a prodrome of Parkinson's disease. *NeuroImage: Clinical*. 2017 Jan 1; 16:313–8.
126. Mole JP, Subramanian L, Bracht T, Morris H, Metzler-Baddeley C, Linden DE. Increased fractional anisotropy in the motor tracts of Parkinson's disease suggests compensatory neuroplasticity or selective neurodegeneration. *European radiology*. 2016 Oct 1; 26(10):3327–35. <https://doi.org/10.1007/s00330-015-4178-1> PMID: 26780637
127. Akram H, Wu C, Hyam J, Foltynie T, Limousin P, De Vita E, Yousry T, Jahanshahi M, Hariz M, Behrens T, Ashburner J. I-Dopa responsiveness is associated with distinctive connectivity patterns in advanced Parkinson's disease. *Movement Disorders*. 2017 Jun; 32(6):874–83. <https://doi.org/10.1002/mds.27017> PMID: 28597560
128. Herz DM, Haagensen BN, Christensen MS, Madsen KH, Rowe JB, Lækkegaard A, Siebner HR. Abnormal dopaminergic modulation of striato-cortical networks underlies levodopa-induced dyskinesias in humans. *Brain*. 2015 Apr 15; 138(6):1658–66.
129. Ng B, Varoquaux G, Poline JB, Thirion B, Greicius MD, Poston KL. Distinct alterations in Parkinson's medication-state and disease-state connectivity. *NeuroImage: Clinical*. 2017 Jan 1; 16:575–85.
130. Forstmann BU, Isaacs BR, Temel Y. Ultra High Field MRI-Guided Deep Brain Stimulation. *Trends Biotechnol*. 2017; 35(10).

131. Isaacs BR, Forstmann BU, Temel Y, Keuken MC. The Connectivity Fingerprint of the Human Frontal Cortex, Subthalamic Nucleus, and Striatum. *Front Neuroanat* [Internet]. 2018; Available from: www.frontiersin.org
132. Lorio S, Fresard S, Adaszewski S, Kherif F, Chowdhury R, Frackowiak RS, et al. New tissue priors for improved automated classification of subcortical brain structures on MRI. *Neuroimage* [Internet]. 2016 Apr 15 [cited 2017 Oct 7]; 130:157–66. Available from: <http://www.ncbi.nlm.nih.gov/pubmed/26854557> <https://doi.org/10.1016/j.neuroimage.2016.01.062> PMID: 26854557
133. Mazziotta JC, Toga AW, Evans AC, Fox P, Lancaster J. A probabilistic atlas of the human brain: theory and rationale for its development. The International Consortium for Brain Mapping (ICBM). *NeuroImage*. 1995.
134. de Hollander G, Keuken MC, Bazin P-L, Weiss M, Neumann J, Reimann K, et al. A gradual increase of iron toward the medial-inferior tip of the subthalamic nucleus. *Hum Brain Mapp* [Internet]. 2014 Sep 1 [cited 2017 Oct 19]; 35(9):4440–9. Available from: <https://doi.org/10.1002/hbm.22485> PMID: 24596026
135. Despotović I, Goossens B, Philips W. MRI segmentation of the human brain: challenges, methods, and applications. *Computational and mathematical methods in medicine*. 2015; 2015.
136. Keuken MC, Isaacs BR, Trampel R, van der Zwaag W, Forstmann BU. Visualizing the human subcortex using ultra-high field magnetic resonance imaging. *Brain topography*. 2018 Jul 1; 31(4):513–45. <https://doi.org/10.1007/s10548-018-0638-7> PMID: 29497874
137. Farhadi F, Vosoughi K, Shahidi GA, Delbari A, Lökk J, Fereshtehnejad SM. Sexual dimorphism in Parkinson's disease: differences in clinical manifestations, quality of life and psychosocial functioning between males and females. *Neuropsychiatric disease and treatment*. 2017; 13:329. <https://doi.org/10.2147/NDT.S124984> PMID: 28203083
138. Smith KM, Dahodwala N. Sex differences in Parkinson's disease and other movement disorders. *Experimental neurology*. 2014 Sep 1; 259:44–56. <https://doi.org/10.1016/j.expneurol.2014.03.010> PMID: 24681088
139. Augustine EF, Pérez A, Dhall R, Umeh CC, Videnovic A, Cambi F, Wills AM, Elm JJ, Zweig RM, Shulman LM, Nance MA. Sex differences in clinical features of early, treated Parkinson's disease. *PloS one*. 2015 Jul 14; 10(7):e0133002. <https://doi.org/10.1371/journal.pone.0133002> PMID: 26171861
140. Keuken MC, Bazin PL, Schäfer A, Neumann J, Turner R, Forstmann BU. Ultra-high 7T MRI of structural age-related changes of the subthalamic nucleus. *Journal of Neuroscience*. 2013 Mar 13; 33(11):4896–900. <https://doi.org/10.1523/JNEUROSCI.3241-12.2013> PMID: 23486960
141. Forstmann BU, Isaacs BR, Temel Y. Ultra High Field MRI-Guided Deep Brain Stimulation. *Trends Biotechnol* [Internet]. 2017; 35(10):904–7. Available from: <https://doi.org/10.1016/j.tibtech.2017.06.010> PMID: 28941469
142. Cochrane CJ, Ebmeier KP. Diffusion tensor imaging in parkinsonian syndromes: a systematic review and meta-analysis. *Neurology*. 2013 Feb 26; 80(9):857–64. <https://doi.org/10.1212/WNL.0b013e318284070c> PMID: 23439701
143. Seppi K, Poewe W. Brain magnetic resonance imaging techniques in the diagnosis of parkinsonian syndromes. *Neuroimaging Clinics*. 2010 Feb 1; 20(1):29–55. <https://doi.org/10.1016/j.nic.2009.08.016> PMID: 19959017